frontiers | Frontiers in Physics

TYPE Original Research
PUBLISHED 14 December 2022
DOI 10.3389/fphy.2022.1076671

Check for updates

OPEN ACCESS

EDITED BY
Weifeng Yang,
Hainan University, China

REVIEWED BY
Vaibhav Prabhudesai,
Tata Institute of Fundamental Research, India
Ladislau Nagy,
Babeş-Bolyai University, Romania

*CORRESPONDENCE
Xinhua Xie,
xinhua.xie@psi.ch

SPECIALTY SECTION
This article was submitted to Optics and Photonics, a section of the journal Frontiers in Physics

RECEIVED 21 October 2022
ACCEPTED 28 November 2022
PUBLISHED 14 December 2022

CITATION
Hu H, Hung Y, Larimian S, Erattupuzha S, Baltuška A, Zeiler M and Xie X (2022), Laser-induced valence electron excitation in acetylene.
Front. Phys. 10:1076671.
doi: 10.3389/fphy.2022.1076671

COPYRIGHT
© 2022 Hu, Hung, Larimian, Erattupuzha, Baltuška, Zeiler and Xie. This is an open-access article distributed under the terms of the Creative Commons Attribution License (CC BY). The use, distribution or reproduction in other forums is permitted, provided the original author(s) and the copyright owner(s) are credited and that the original publication in this journal is cited, in accordance with accepted academic practice. No use, distribution or reproduction is permitted which does not comply with these terms.

Laser-induced valence electron excitation in acetylene

Hongtao Hu[1], Yi Hung[1], Seyedreza Larimian[1], Sonia Erattupuzha[1], Andrius Baltuška[1], Markus Zeiler[1] and Xinhua Xie[2]*

[1]Photonics Institute, Technische Universität Wien, Vienna, Austria, [2]SwissFEL, Paul Scherrer Institute, Villigen, Switzerland

Strong-field induced valence electron excitation is a common process in strong field interaction with atoms and molecules. In the case of polyatomic molecules, the effects of ionization from low-lying molecular orbitals and nuclear dynamics during the interaction can play critical roles for electron excitation. In this work, we investigate the involved molecular orbitals in the electron excitation of singly ionized acetylene in a strong laser field using alignment dependence and laser intensity dependence. Additionally, the involved nuclear dynamics during the electron excitation are identified from the difference in the kinetic energy release and the angular distribution of laser-induced dissociation with different pulse durations and intensities. The laser intensity dependence clearly shows the relative strength change of two excitation pathways in the measured momentum and angle-resolved distributions.

KEYWORDS

electron excitation, strong laser field, molecular dissociation, nuclear dynamics, strong-field ionization, tunneling ionization

Introduction

The ultrafast dynamics of valence electrons play essential roles in the properties and reaction behaviors of atoms and molecules [1]. In general, the valence electron dynamics happens on a time scale of sub-femtosecond or attosecond. Therefore, laser-induced molecular dynamics involving valence electron excitation is of general interest in strong field and attosecond sciences [2]. In a strong laser field, its electric field strength can be equivalent to the Coulomb potential field of valence electrons. When a molecule is exposed to such a laser field, valence electrons can be released through strong-field ionization [3]. After ionization, the electron density of the molecules will be redistributed on a time scale of femtoseconds or sub-femtoseconds and the geometry of the molecule will change to find a new equilibrium accordingly. In many cases, the molecule will become unstable, which leads to the breakage of chemical bonds through molecular dissociation, or the formation of new chemical bonds through molecular isomerization [4–7]. Most of such laser-induced molecular reactions involve electronically excited states. Therefore, valence electron excitation is critical for studies of laser-induced molecular reactions.

Previous experiments demonstrated that there exist several different mechanisms for strong-field electron excitation connected with strong-field ionization. In general, in these experiments, the driving laser field is a non-resonant field with respect to the molecular energy level structure. The four most common processes are 1) electron excitation through laser-induced strong-field ionization from low-lying molecular orbitals [5, 8–13]; 2) electron excitation through laser-induced electron rescattering after strong-field ionization [14–17]; 3) laser-induced electron excitation through single- or multi-photon transitions after strong-field ionization (so-called bond softening process) [18–21]; and 4) laser-induced electron recapture to electron excited states after strong-field ionization [22–25]. All four electron excitation processes start with strong-field ionization.

One important feature of molecular strong-field ionization in a strong laser field is that the ionization rate depends on the angle between the molecular axis and the laser polarization direction [5, 13, 26–29]. The angular ionization probability of a molecule is determined by the shape and symmetry of the involved molecular orbitals [30]. For example, strong-field ionization of electrons from the HOMO of C_2H_2, a π-orbital, reaches a maximum when the laser is polarized perpendicular to the molecular axis, while for the ionization from a σ-orbital, the maximum ionization probability appears when the laser polarization direction is parallel to the molecular axis [5]. Therefore, using the angular dependence of strong-field ionization, we could determine the contributions from certain molecular orbitals in experiments [13].

The laser pulse duration is one of the critical parameters in strong field interaction [21, 31–33]. In the case of molecules, nuclear dynamics can be involved during the interaction. Previous studies showed that the so-called bond-softening process in H_2 can be strongly suppressed when using laser pulses with a pulse duration of shorter than 10 fs [21]. Within a short pulse, the effect of nuclear motion can be minimized because nuclear dynamics is much slower than electron dynamics. Therefore, using the dependence on pulse duration, we can possibly identify the effect from nuclear dynamics.

In this work, using C_2H_2 as an example, we investigate the electron excitation of polyatomic molecules in a strong laser field. We exploit the ionization and dissociation signals of pre-aligned C_2H_2 in a strong laser field with two different pulse durations to reveal the involved molecular orbitals and nuclear dynamics in electron excitation processes.

Experiment

In the experiment, we use a Cold Target Recoil Ion Momentum Spectroscopy (COLTRIMS) apparatus to measure charged particles (electrons and ions) from the laser-molecule interaction [16, 34, 35] with 800 nm and 25 fs laser pulses from a Ti:Sapphire amplifier. From the measurements, we identify non-dissociative and dissociative processes after single and double ionization of C_2H_2. In this work, we focus on electron excitation after single ionization. Figure 1A shows the measured ion signal distribution over the time-of-flight and x position on the detector. In the distribution, non-dissociative ionization signals ($C_2H_2^+$ and its isotopic species) appear as sharp spots, while ion signals (C_2H^+) from dissociation exhibit a broader ring-like or plate-like distribution due to the energy released from the chemical bond breakage. As marked in the figure, we can distinguish the $C_2H_2^+$ signal from non-dissociative and dissociative single ionization. It is to be noted that large ring-like signals belong to the dissociation of doubly ionized $C_2H_2^{2+}$, which is confirmed using two-body coincidence detection of C_2H^+ and H^+.

The molecular axes of molecules in the gas phase are, in general, randomly aligned. When the molecules are exposed to a strong and short laser pulse, they can be aligned through so-called impulsive laser alignment [36]. For the alignment measurements, we split the laser beam into an ionization beam and an alignment beam with a beam splitter. Both beams are linearly polarized along the same direction. The peak intensity of the alignment beam at the focus is below 1×10^{13} W/cm^2 to excite a rotational wave packet in the molecule [36], while the ionization beam with a peak intensity of 4×10^{14} W/cm^2 arrives at the target with a certain time delay controlled by a motorized linear stage. The laser peak intensity is calibrated with the time-of-flight spectrum of H_2 [37]. As shown in Figure 1B, the rotational revival structures are presented in the measured $C_2H_2^{2+}$ signal over the time delay between the alignment and the ionization pulse. In the same figure, we also plot the calculated the alignment quality of C_2H_2, the expectation value to $\cos^2\theta$ with θ the angle between the molecule axis and the laser polarization direction [5]. The measured ion signals overall follow the structures in the simulated data, except for a phase-flip which is introduced by the ionization process from the HOMO of C_2H_2 [5].

To achieve 4.5 fs laser pulses for the short pulse measurement, the ionization beam is focused into a gas-filled hollow capillary in which its spectrum is broadened [38]. After re-collimation, the beam is compressed with chirped mirrors, and a wedge pairs down to 4.5 fs[39]. The pulse duration of the ionization pulses is characterized by a stereo-ATI device [39, 40].

Results and discussions

KER distributions

Since the ground state of $C_2H_2^+$ is metastable and the excited states of $C_2H_2^+$ are mostly dissociative [5], in the experiment, we used the dissociation from single ionization to study the electron excitation of $C_2H_2^+$. In this work, we focus on the dissociation of

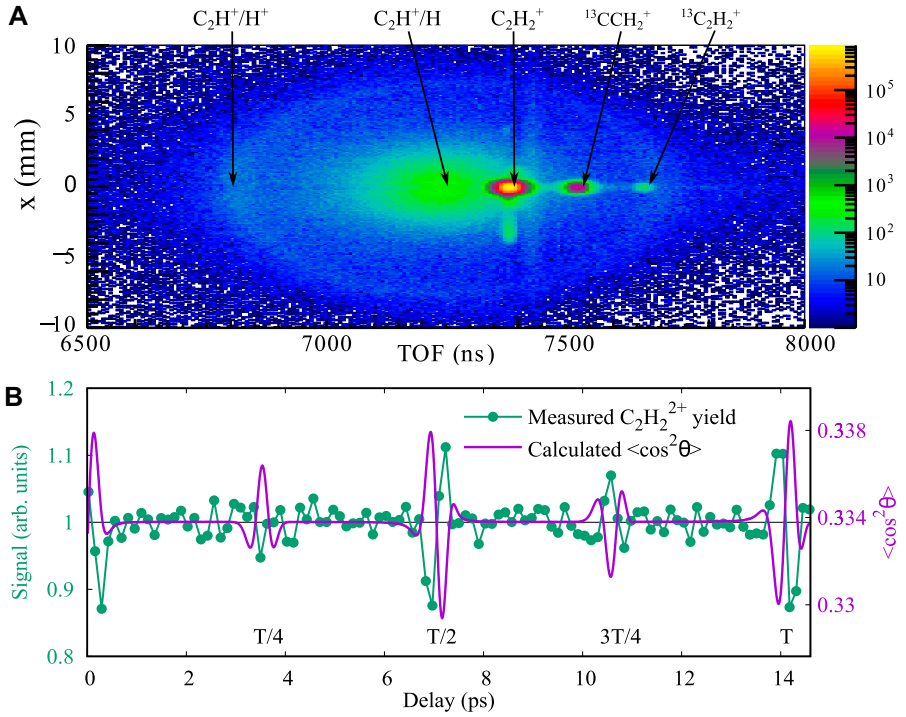

FIGURE 1
(A) Measured ion count distribution over the time-of-flight and x position on the detector. The peak intensity of the laser field is 4×10^{14} W/cm^2, and the pulse duration is 25 fs. **(B)** Measured $C_2H_2^{2+}$ signal and simulated $<\cos^2\theta>$ as a function of the time delay between the alignment and the ionization pulse. For the simulation, the gas temperature of 200 K and the peak intensity of 1×10^{13} W/cm^2 of the alignment pulse are used.

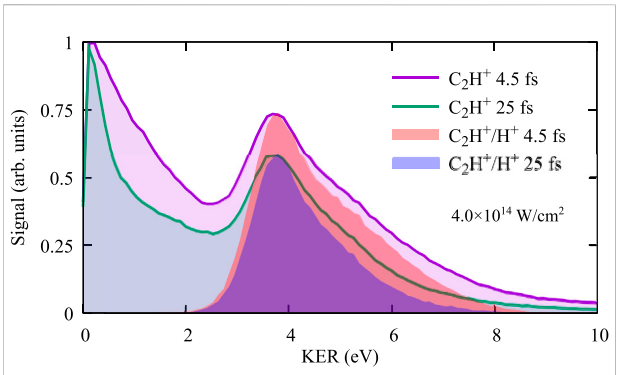

FIGURE 2
Measured KER distributions of laser-induced C-H dissociation for the pulse duration of 4.5 fs and 25 fs, selected with a single C_2H^+ ion and with the two-body coincidence detection of C_2H^+ and H^+.

the C-H bond breakage after single ionization, in which the nuclear dynamics is faster than that of the C-C bond breakage. Using momentum conservation, we calculate the kinetic energy released (KER) with the measured momentum of C_2H^+ through $E_{KER} = p^2_{C_2H}(1/m_{C_2H} + 1/m_H)/2$. In Figure 2, we depict the KER distributions for the two pulse durations with all C_2H^+ signals. The KER distributions show one peak close to zero and another at about 3.8 eV. In the figure, we include also the KER distributions of the two-body fragmentation (C_2H^+/H^+) from double ionization, which exhibit a peak at 3.8 eV. It is clear that the high energy peak of the measured KER with dominant C_2H^+ signals comes from the dissociation of doubly ionized molecules, while the lower energy signals with energy lower than 2 eV are dominantly from the dissociation after single ionization. Thus, we can separate the dissociation signal of single ionization from double ionization. The discrepancies at large energies between the KER distributions from two-body coincidence selection and those from one ion selection are due to the overlap with background water (H_2O^+) signals which are excluded in the coincidence selection. The relative strength of the background signal is sensitive to the gas density and the laser focusing conditions.

Alignment dependence

Comparing the results between 4.5 fs and 25 fs for the dissociation after single ionization in Figure 2, we find that the KER distribution of the measurement with 4.5 fs pulses is

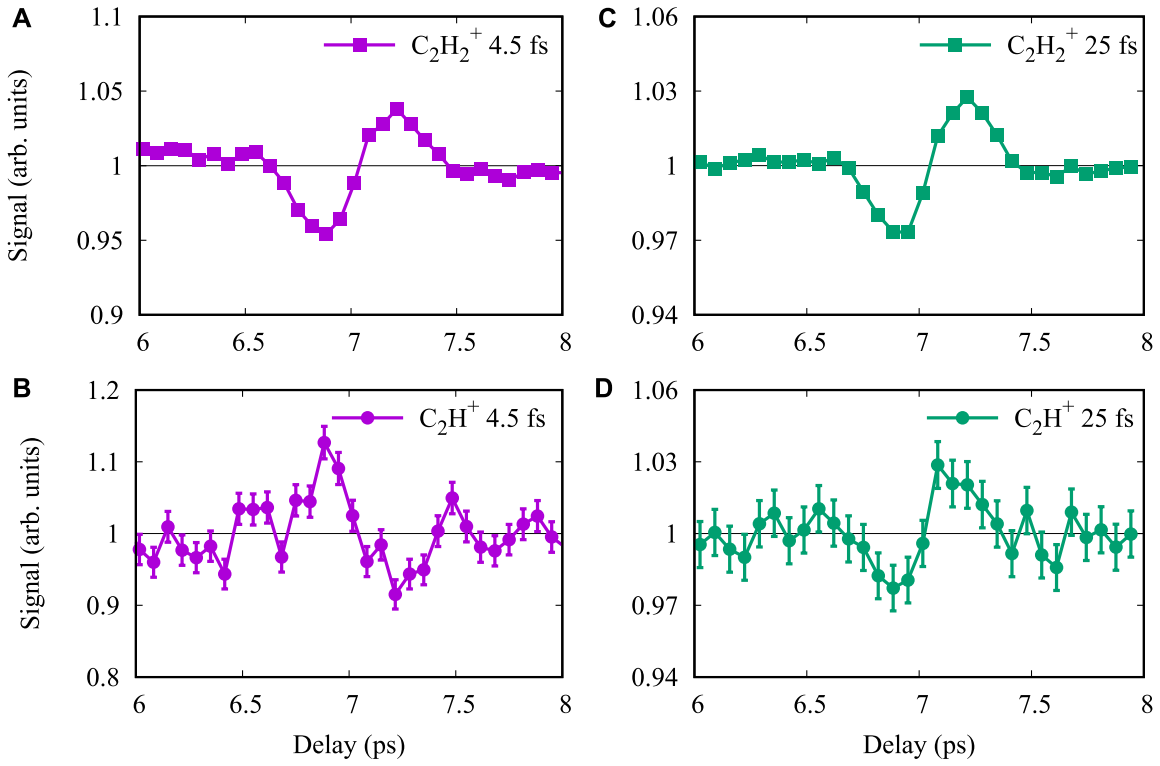

FIGURE 3
Measured ion signals as a function of the time delay between the alignment and the ionization pulse around the half rotational revival. Panels **(A,C)** are for the signals of non-dissociative $C_2H_2^+$, while **(B,D)** are those for the dissociative of $C_2H_2^+$ to C_2H^+/H. The measurements with pulse durations of 4.5 fs and 25 fs are shown in **(A,B)** and **(C,D)**, respectively. The laser peak intensity is 4 × 10^{14} W/cm^2 for both measurements.

broader, which means more high-energy signals than those with 25 fs Since 4.5 fs pulses have a much broader bandwidth than 25 fs laser pulses, an intuitive explanation for the width difference in the KER distributions could be the bandwidths of the driven laser pulses. However, due to the momentum conservation for the ejected electron and the rest of the molecule, the energy gained from the laser field will be mostly carried by the electron due to the significant mass difference between the electron and the ion. Therefore, the kinetic energy release of laser-induced molecular dissociation has minor influence from the laser bandwidth but is rather determined by the initial distribution of the nuclear wave packet and the slope of the involved potential energy surfaces. The difference in KER implies involving of different nuclear dynamics during the dissociation process. To understand the beneath physical mechanism, we further analyze the data of alignment measurements with the selection of KER less than 2 eV for the dissociation of C_2H_2 after single ionization.

For the alignment dependence, we focus on signals around the half-rotational revival, during which the molecules are first aligned parallely at a delay time of 6.8 ps and afterward perpendicular to the laser polarization direction at a delay time of 7.2 ps. Figures 3A,B show the ion signals of non-dissociative and dissociative single ionization of C_2H_2 around the half-rotation revival for the measurement with 4.5 fs ionization pulses. As has been reported previously, for 4.5 fs laser pulses, the $C_2H_2^+$ signal has a maximum at the perpendicular alignment because of ionization from the HOMO, while the C_2H^+ signal shows an opposite dependence on the alignment with the major contribution to ionization from HOMO-2 [5].

Figures 3C,D depict the ion signals for the measurement with 25 fs ionization pulses. The $C_2H_2^+$ signal over the pump-probe delay is similar to that with 4.5 fs laser pulses, which indicates dominant ionization from HOMO as well. However, the C_2H^+ signal with 25 fs exhibits an opposite dependence on the alignment from that with 4.5 fs: the peak signal appears at the perpendicular alignment of the molecular axis to the direction of the laser polarization. Such dependence is the same as the $C_2H_2^+$ and infers that the strong-field ionization is dominantly from HOMO.

Laser-induced electron excitation mechanics

To understand the dependence on laser pulse duration, we draw the potential energy curves of C_2H_2 over the C-H coordination in Figure 4. The removal of a HOMO electron

10.3389/fphy.2022.1076671

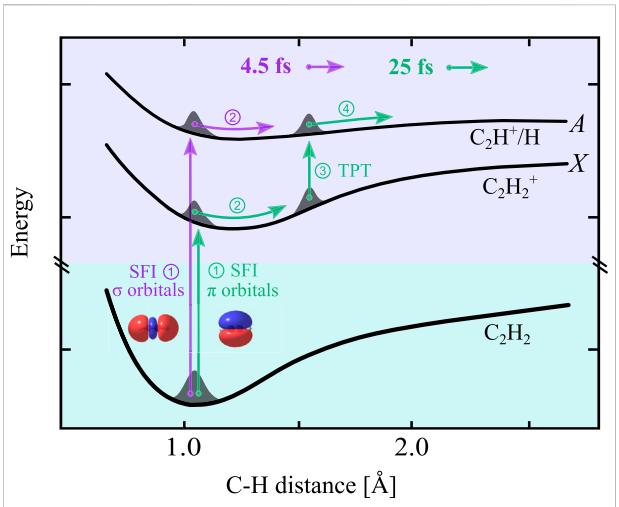

FIGURE 4
Schematic view of electron excitation of C_2H_2 in a strong laser field. Two pathways are represented with arrows of different colors. The HOMO-2 pathway: for the interaction with a short laser pulse with a pulse duration shorter than the C-H vibrational period, strong field ionization (SFI) of a HOMO-2 electron directly leads to the electronically excited and dissociative A state. The HOMO pathway: for the interaction with a long laser pulse with a pulse duration longer than the C-H vibrational period, first, an electron is removed from the HOMO which launches a vibrational wave packet on the potential surface of the $C_2H_2^+$ ground state. The vibrational wave packet moves toward a larger C-H distance and resonant three-photon transition (TPT) occurs once the energy gap fits the energy of three 800-nm photons. The potential energy curves are adapted from Ref. [5].

brings the molecule into the ground state of the cation (X state), and the removal of a HOMO-2 electron directly prompts the molecule into the lowest electronic excited state (A state) of the cation, which is dissociative over the C-H coordination. There are two possible pathways to reach the A state from a neutral C_2H_2. The first one is strong-field ionization directly from HOMO-2. The second one happens sequentially through first reaching the X-state through the removal of a HOMO electron and then a HOMO-2 electron being excited to the hole in the HOMO formed through ionization. The measured signal of $C_2H_2^+$ over alignment pump-probe delays show a clear signature of strong-field ionization of a HOMO electron for both laser pulse durations. On the other hand, the dissociative single ionization shows opposite behavior on the molecular alignment, which refers that the involved ionization and excitation processes are not the same.

In the case of 4.5 fs laser pulses, the C-H coordinate can be treated as frozen during the laser interaction, and therefore, the ionization happens dominantly at the Franck–Condon region. The measured results, shown in Figure 3B, indicate that the population of the dissociative channel is dominated by direct ionization from HOMO-2, which exhibits a peak signal at the parallel alignment. However, the scenario of the dissociation with 25 fs laser pulses is different. The measured results in Figure 3 D show dependence on the alignment from the ionization of a HOMO electron. As we mentioned, with the ionization of a HOMO electron, the molecule ends at the stable X state of the cation. Therefore, to reach the A state, further actions are necessary to excite the cation. After the strong-field ionization at around the peak of the laser field, the tail of the laser pulse can still have actions on the molecule. There are several possible ways to excite an electron from the HOMO-2 to HOMO to reach the A state. The first one is excitation through electron rescattering: the removed HOMO electron is accelerated in the laser field and can be driven back and scattered with its parent. Such electron rescattering can either kick out or excite a second electron, depending on the rescattering energy. In our experimental condition with a peak intensity of 4×10^{14} W/cm^2, the rescattering energy can be as high as 76 eV, which is sufficient to excite $C_2H_2^+$ from the X state to the A state. This energy difference in the distribution also rules out the major contribution from electron rescattering. For an electron rescattering process, the scattering mainly happens within one optical cycle of the laser field which is 2.7 fs. In such a short time scale, the stretching of the C-H bond is minor. Therefore, the nuclear wave packet populated on the A state is still approximately the Franck–Condon region, which shall lead to a similar energy distribution as the direct ionization from HOMO-2.

The second possible pathway is molecular dissociation involving nuclear dynamics, similar to the bond softening in the dissociation of H_2^+ in a strong laser field [18]. In the first step, one electron is released from HOMO at the Franck–Condon region, and the ion ends at the X state with vibrational excitation. The C-H stretching of $C_2H_2^+$ can occur on a fast time scale with a vibrational period of 10.3 fs for asymmetric stretching and 10.6 fs for symmetric stretching [41]. Therefore, when the laser pulse has pulse duration longer than the vibrational period, the nuclear wave packet on the X state can move toward the new equilibrium geometry through the stretching of the C-H bond within the laser pulse. The energy gap between the X and A states is about 5.4 eV which is away from the multi-photon resonance of 800 nm [42, 43]. Along the stretching, the energy gap between the X state and the A state changes as well. The transition from the X state to the A state occurs once the energy gap becomes the three-photon resonance (4.65 eV) of 800-nm photons. After the transition, dissociation from the A state happens with a slightly lower dissociation energy, as shown in Figure 4. Comparing the distribution in the low energy between measurements with the two pulse durations, we notice that the energy edge shifted to the higher value by about 0.5 eV for the 4.5 fs at the half maximum. This observation is direct evidence that the initial nuclear wave packet is at a different position on the potential energy surface, and it supports the bond-softening scenario for the 25 fs case.

On the other side, when the laser pulse duration is 4.5 fs, it is much shorter than the C-H vibrational period. After single ionization, the laser field drops off rapidly before significant stretching of the C-H bond, which prevents the multiphoton transition at a large C-H distance. Therefore, the excitation to the

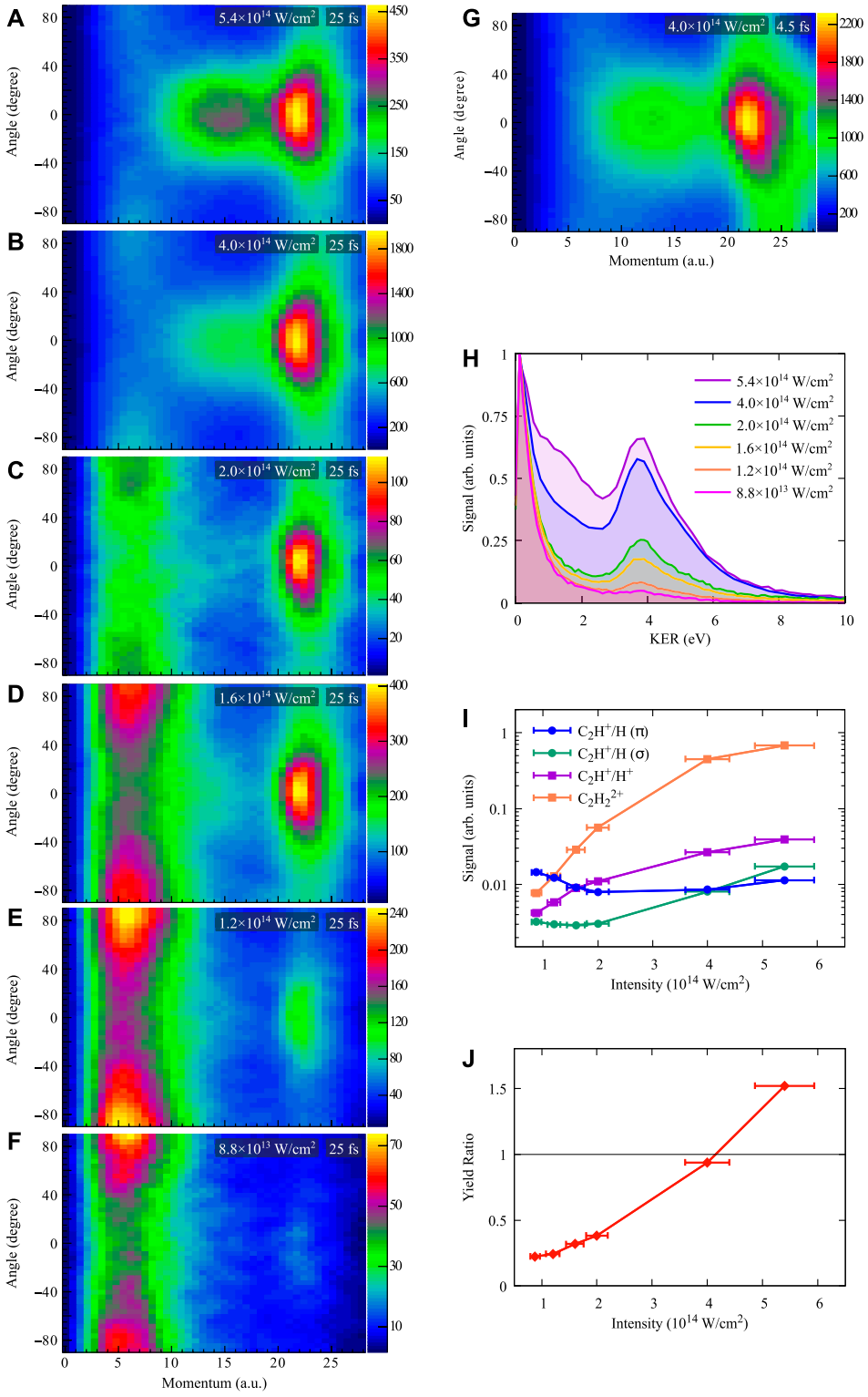

FIGURE 5
Measured ion signal distributions over the momentum and the angle to the laser polarization direction for different laser peak intensities with the pulse duration of 25 fs**(A–F)** and 4.5 fs **(G)**. **(H)** Normalized kinetic energy distributions of the molecular dissociation for different laser peak intensities with the pulse duration of 25 fs. **(I)** Ion yields for different ionization and dissociation channels over laser intensity normalized to the non-dissociative single ionization signal ($C_2H_2^+$). **(J)** The ion yield ratio between the direct (HOMO-2) and indirect (HOMO) dissociative single ionization over laser intensity.

A state is dominant by direct ionization from HOMO-2, and the dissociation ends with a higher KER than that of a bond-softening pathway.

As mentioned, there is one more possible way for valence electron excitation, which is electron recapture after strong-field ionization [22, 24, 25]. Electron recapture after double ionization will lead to singly ionized C_2H_2. It will lead to either stable high-lying Rydberg states of $C_2H_2^+$ or dissociation of $C_2H_2^+$. In case of dissociation, the KER will be similar to that from doubly ionized due to the weak screening effect from the high-lying Rydberg electron to the molecular dissociation of C_2H_2 [23, 44]. Therefore, the signals induced by electron recapture have no contribution to the measured dissociation signals of single ionization with a KER less than 2 eV.

Dependence on laser intensity

Strong laser field-induced molecular ionization and dissociation are highly non-linear processes; therefore, laser intensity is a critical parameter for these processes. For the electron excitation process of singly ionized C_2H_2, both the strong-field ionization and possible transition between two electronic states are sensitive to the laser intensity which shall lead to laser intensity dependence. To demonstrate such dependence, we perform measurements with different laser peak intensities in the range from 8.8×10^{13} to 5.4×10^{14} W/cm^2 with a pulse duration of 25 fs. In the data analysis for the dependence on laser intensity, we integrate signals with all delays between the alignment and the ionizing pulses, with, therefore, no preferential alignment of the molecules. Figure 5H presents the normalized KER distributions for six laser peak intensities. With the increase of the laser peak intensity, the dissociative double ionization signals peaking at 3.8 eV increase monotonically, and the signals around 2 eV increase as well. From the experiment, we obtain three-dimensional momentum vectors of ions. Therefore, in addition to the KER (or momentum) distribution, angular distributions of ions can be derived from the momentum vectors. In Figures 5A–G, we plot the two-dimensional ion (C_2H^+) signal distributions over the momentum ($p_r = \sqrt{p_x^2 + p_y^2 + p_z^2}$) and the angle to the laser polarization direction ($\theta = \tan^{-1}(p_y/p_z)$) for different intensities.

First, let us focus on the distribution at one certain intensity. For instant, in Figure 5B, with the laser peak intensity of 4×10^{14} W/cm^2 and the pulse duration of 25 fs, we can identify three different regions from the distribution: the first region with momentum less than 9 a.u. (KER < 0.6 eV), the second region with momentum larger than 9 a.u. but less than 19 a.u. (0.6 < KER < 2.8 eV), and the third region with momentum larger than 19 a.u. (KER > 2.8 eV). We know that the first and second regions are dissociation signals after single ionization, while the third region originates from double ionization, according to Figure 2. Since the ion ejected along the molecular axis, the measured angle θ represents the molecular axis to the laser polarization direction. For the first region, the angular distribution exhibits a minimum at 0° (parallel to the laser polarization direction) and maxima at ±90° (perpendicular to the laser polarization direction). Such angular distribution indicates strong-field ionization from a π orbital (HOMO) has peak ionization probability when the molecular axis is perpendicular to the laser polarization direction, which is consistent with the findings from the alignment dependence. On the other hand, the angular distribution for the third region (C_2H^+/H^+) shows an opposite behavior, maximum at 0° and minima at ±90°, which indicates at least one electron removed from HOMO-2 σ orbital [5]. We notice that the angular distribution for the second region ($9 < p_r < 19$ a.u.) is different from the first and third regions. The distribution displays maximum at 0° and minima at ±90°, which is opposite to that of the first region and similar to that of the third region but with a narrower distribution. Such distribution implies single ionization from the HOMO-2 which has a maximum ionization probability when the molecular axis is parallel to the laser polarization direction. One previous study on the dissociation from double ionization [5] demonstrated double ionization leading to the C_2H^+/H^+ channel involves one HOMO and one HOMO-2 electron. The convolution of the ionization probability from the HOMO and HOMO-2 broadens the angular distribution and, therefore, yields broader distribution than that of single ionization with one HOMO-2 electron (the second region).

Figure 5G shows the two-dimensional angle-momentum distribution for the same peak intensity but with a pulse duration of 4.5 fs. To compare with the distribution of 25 fs in Figure 5B, the overall structures are similar but the relative signal strength in the three regions are different and with broader angular distributions for the second and third regions. This observation also explains the difference in the KER distributions shown in Figure 2. More signals in the second region for the measurement with 4.5 fs pulses lead to a broader KER distribution for the dissociation of singly ionized C_2H_2. As discussed previously, for the case of 4.5 fs, the dissociation from single ionization happens dominantly from the direct removal of a HOMO-2 electron, which agrees with maximum signals at 0° in the angular distribution for the second region. The narrower angular distributions in the second and third regions for the pulse duration of 25 fs can be explained by the laser-induced alignment after strong-field ionization [45], which has been previously observed in C_2H_4 experiments [6].

In the angle–momentum distributions, we can explicitly identify two pathways with different momentum and angular distributions for the molecular dissociation after single ionization from HOMO and HOMO-2: ionization from HOMO leads to dominant signals at the perpendicular direction with momentum less than 9 a.u. (KER < 0.6 eV) and ionization from HOMO-2 yields dominant signals at the parallel direction with momentum larger than 9 a.u. and less than 19 a.u. ((0.6 < KER < 2.8 eV)).

Such behaviors agree well with the findings in the alignment experiments and support the proposed direct (ionization from HOMO-2) and indirect (bond-softening after ionization from HOMO) electron excitation mechanisms.

Now, let us continue to the dependence of the laser-induced dissociation on the laser intensities with the pulse duration of 25 fs. Figures 5A–F reveal that the dominant dissociation signals from single ionization shift from the first region to the second region with the increasing of the peak intensity from 8.8×10^{13} to 5.4×10^{14} W/cm^2, while the dissociation signals from double ionization increase monotonically. To quantify the dependence on the laser peak intensity, we integrate the signals in the three regions and compare them with the yields of non-dissociative single ($C_2H_2^+$) and double ($C_2H_2^{2+}$) ionization. Figure 5I illustrates the ion yields which are normalized to that of non-dissociative single ionization ($C_2H_2^+$). In the plot, we note that the dissociative (C_2H^+/H^+) and non-dissociative ($C_2H_2^{2+}$) double ionization yields monotonically increase along the increasing of the laser peak intensity and approach saturation at the peak intensity of 5.4×10^{14} W/cm^2. On the other hand, the two pathways of dissociation from single ionization (C_2H^+/H) exhibit different intensity dependence. The signals from the ionization of HOMO (π orbital) first decrease in the low-intensity regime and increase again in the high-intensity regime. This behavior can be explained by the interplay between the depletion of the single ionization to higher charge states with the increasing of laser intensities and the focal volume effect. The signals from the ionization of HOMO-2 (σ orbital) stay on a low level when the peak intensity is below 2×10^{14} W/cm^2, and when the intensity is above this level, the signals start to increase. The ratio between the yield of the two pathways is depicted in Figure 5J, which represents the increase of the HOMO-2 (σ orbital) pathway with respect to the HOMO (π orbital) pathway with a significant increase from 0.2 to 1.5. The HOMO pathway is dominant in the low-intensity regime, but when the intensity increases to above 5×10^{14} W/cm^2, the HOMO-2 pathway becomes stronger.

These results show that not only the absolute yields but also the relative yields of molecular dissociation between different pathways strongly depend on the laser intensity. Therefore, together with the pulse duration and the molecular alignment, the laser intensity can be used as an effective knob to control the laser-induced electron excitation and following molecular dissociation.

Conclusion

In conclusion, we experimentally distinguished the two dominant electron excitation pathways in single ionization of C_2H_2 by strong laser fields. With the alignment dependence of the dissociation signal, we could determine the involved molecular orbitals in the electron excitation. Additionally, the influence of nuclear dynamics after ionization can be identified from the dependence of the dissociation KER on the pulse duration and the intensity of the ionizing laser pulse. The observed electron excitation processes in C_2H_2 can be general in polyatomic molecules since strong-field ionization from low-lying molecular orbital is not a rare process, and nuclear dynamics on the 10 femtosecond timescale, within the duration of laser pulses used in many experiments, takes place in many molecules, in particular those containing C-H bonds. Moreover, the momentum and angle-resolved distributions contain information on both the orbital from which an electron is released and the nuclear dynamics happening during strong-field interaction. In turn, these distributions provide information on the ultrafast electron and nuclear dynamics in polyatomic molecules taking place during and after strong-field ionization.

Data availability statement

The raw data supporting the conclusions of this article will be made available by the authors, without undue reservation.

Author contributions

SL, SE, MZ, and XX conducted the experiment. YH, HH, and XX analyzed the data. All co-authors contributed to the discussion and writing of the manuscript.

Funding

This work was supported by Austrian Science Fund (FWF) under P30465-N27 and ZK 9100-N. Open access funding provided by PSI - Paul Scherrer Institute.

Conflict of interest

The authors declare that the research was conducted in the absence of any commercial or financial relationships that could be construed as a potential conflict of interest.

Publisher's note

All claims expressed in this article are solely those of the authors and do not necessarily represent those of their affiliated organizations, or those of the publisher, the editors, and the reviewers. Any product that may be evaluated in this article, or claim that may be made by its manufacturer, is not guaranteed or endorsed by the publisher.

References

1. Kauzmann W. *Quantum chemistry: An introduction*. Amsterdam, Netherlands: Elsevier (2013).

2. Corkum PB, Krausz F. Attosecond science. *Nat Phys* (2007) 3:381–7. doi:10.1038/nphys620

3. Augst S, Strickland D, Meyerhofer DD, Chin SL, Eberly JH. Tunneling ionization of noble gases in a high-intensity laser field. *Phys Rev Lett* (1989) 63: 2212–5. doi:10.1103/physrevlett.63.2212

4. Posthumus JH. The dynamics of small molecules in intense laser fields. *Rep Prog Phys* (2004) 67:623–65. doi:10.1088/0034-4885/67/5/r01

5. Xie X, Doblhoff-Dier K, Xu H, Roither S, Schöffler MS, Kartashov D, et al. Selective control over fragmentation reactions in polyatomic molecules using impulsive laser alignment. *Phys Rev Lett* (2014) 112:163003. doi:10.1103/PhysRevLett.112.163003

6. Xie X, Roither S, Schöffler M, Lötstedt E, Kartashov D, Zhang L, et al. Electronic predetermination of ethylene fragmentation dynamics. *Phys Rev X* (2014) 4:021005. doi:10.1103/PhysRevX.4.021005

7. Hartmann N, Bhattacharyya S, Schlaepfer F, Volkov M, Schumacher Z, Lucchini M, et al. Ultrafast nuclear dynamics of the acetylene cation C2H2+ and its impact on the infrared probe pulse induced C-H bond breaking efficiency. *Phys Chem Chem Phys* (2019) 21:18380–5. doi:10.1039/C9CP03138C

8. Yao J, Li G, Jia X, Hao X, Zeng B, Jing C, et al. Alignment-dependent fluorescence emission induced by tunnel ionization of carbon dioxide from lower-lying orbitals. *Phys Rev Lett* (2013) 111:133001. doi:10.1103/PhysRevLett.111.133001

9. Erattupuzha S, Larimian S, Baltuška A, Xie X, Kitzler M. Two-pulse control over double ionization pathways in CO2. *J Chem Phys* (2016) 144:024306. doi:10.1063/1.4939638

10. Farrell JP, Petretti S, Förster J, McFarland BK, Spector LS, Vanne YV, et al. Strong field ionization to multiple electronic states in water. *Phys Rev Lett* (2011) 107:083001. doi:10.1103/PhysRevLett.107.083001

11. Akagi H, Otobe T, Staudte A, Shiner A, Turner F, Dörner R, et al. Laser tunnel ionization from multiple orbitals in hcl. *science* (2009) 325:1364–7. doi:10.1126/science.1175253

12. Wu C, Zhang H, Yang H, Gong Q, Song D, Su H. Tunneling ionization of carbon dioxide from lower-lying orbitals. *Phys Rev A* (2011) 83:033410. doi:10.1103/PhysRevA.83.033410

13. Hu H, Kangaparambi S, Dorner-Kirchner M, Hanus V, Baltuška A, Kitzler-Zeiler M, et al. Quantitative retrieval of the angular dependence of laser-induced electron rescattering in molecules. *Phys Rev A* (2021) 103:013114. doi:10.1103/PhysRevA.103.013114

14. Kopold R, Becker W, Rottke H, Sandner W. Routes to nonsequential double ionization. *Phys Rev Lett* (2000) 85:3781–4. doi:10.1103/PhysRevLett.85.3781

15. Feuerstein B, Moshammer R, Fischer D, Dorn A, Schröter CD, Deipenwisch J, et al. Separation of recollision mechanisms in nonsequential strong field double ionization of ar: The role of excitation tunneling. *Phys Rev Lett* (2001) 87:043003. doi:10.1103/PhysRevLett.87.043003

16. Xie X, Roither S, Kartashov D, Persson E, Arbó DG, Zhang L, et al. Attosecond probe of valence-electron wave packets by subcycle sculpted laser fields. *Phys Rev Lett* (2012) 108:193004. doi:10.1103/PhysRevLett.108.193004

17. Endo T, Matsuda A, Fushitani M, Yasuike T, Tolstikhin OI, Morishita T, et al. Imaging electronic excitation of no by ultrafast laser tunneling ionization. *Phys Rev Lett* (2016) 116:163002. doi:10.1103/PhysRevLett.116.163002

18. Bucksbaum PH, Zavriyev A, Muller HG, Schumacher DW. Softening of the H2+ molecular bond in intense laser fields molecular bond in intense laser fields. *Phys Rev Lett* (1990) 64:1883–6. doi:10.1103/PhysRevLett.64.1883

19. Zavriyev A, Bucksbaum PH, Muller HG, Schumacher DW. Ionization and dissociation ofH2in intense laser fields at 1.064 μm, 532 nm, and 355 nm. *Phys Rev A* (1990) 42:5500–13. doi:10.1103/PhysRevA.42.5500

20. Giusti-Suzor A, He X, Atabek O, Mies FH. Above-threshold dissociation of H2+ in intense laser fieldsnse laser fields. *Phys Rev Lett* (1990) 64:515–8. doi:10.1103/PhysRevLett.64.515

21. McKenna J, Anis F, Sayler AM, Gaire B, Johnson NG, Parke E, et al. Controlling strong-field fragmentation of H2+ by temporal effects with few-cycle laser pulses. *Phys Rev A* (2012) 85:023405. doi:10.1103/physreva.85.023405

22. Nubbemeyer T, Gorling K, Saenz A, Eichmann U, Sandner W. Strong-field tunneling without ionization. *Phys Rev Lett* (2008) 101:233001. doi:10.1103/PhysRevLett.101.233001

23. Manschwetus B, Nubbemeyer T, Gorling K, Steinmeyer G, Eichmann U, Rottke H, et al. Strong laser field fragmentation ofH2: Coulomb explosion without double ionization. *Phys Rev Lett* (2009) 102:113002. doi:10.1103/physrevlett.102.113002

24. Larimian S, Erattupuzha S, Lemell C, Yoshida S, Nagele S, Maurer R, et al. Coincidence spectroscopy of high-lying rydberg states produced in strong laser fields. *Phys Rev A* (2016) 94:033401. doi:10.1103/PhysRevA.94.033401

25. Larimian S, Erattupuzha S, Baltuška A, Kitzler-Zeiler M, Xie X. Frustrated double ionization of argon atoms in strong laser fields. *Phys Rev Res* (2020) 2: 013021. doi:10.1103/PhysRevResearch.2.013021

26. Alnaser AS, Maharjan CM, Tong XM, Ulrich B, Ranitovic P, Shan B, et al. Effects of orbital symmetries in dissociative ionization of molecules by few-cycle laser pulses. *Phys Rev A* (2005) 71:031403. doi:10.1103/PhysRevA.71.031403

27. Śpiewanowski MD, Madsen LB. Alignment- and orientation-dependent strong-field ionization of molecules: Field-induced orbital distortion effects. *Phys Rev A* (2015) 91:043406. doi:10.1103/PhysRevA.91.043406

28. Zeidler D, Staudte A, Bardon AB, Villeneuve DM, Dörner R, Corkum PB. Controlling attosecond double ionization dynamics via molecular alignment. *Phys Rev Lett* (2005) 95:203003. doi:10.1103/PhysRevLett.95.203003

29. Lam HVS, Yarlagadda S, Venkatachalam A, Wangjam TN, Kushawaha RK, Cheng C, et al. Angle-dependent strong-field ionization and fragmentation of carbon dioxide measured using rotational wave packets. *Phys Rev A* (2020) 102: 043119. doi:10.1103/PhysRevA.102.043119

30. Tong XM, Zhao ZX, Lin CD. Theory of molecular tunneling ionization. *Phys Rev A* (2002) 66:033402. doi:10.1103/physreva.66.033402

31. Reischl B, de Vivie-Riedle R, Rutz S, Schreiber E. Ultrafast molecular dynamics controlled by pulse duration: The na3 molecule. *J Chem Phys* (1996) 104:8857–64. doi:10.1063/1.471620

32. Bocharova I, Karimi R, Penka EF, Brichta JP, Lassonde P, Fu X, et al. Charge resonance enhanced ionization of CO2 probed by laser Coulomb explosion imaging. *Phys Rev Lett* (2011) 107:063201. doi:10.1103/PhysRevLett.107.063201

33. Xie X, Lötstedt E, Roither S, Schöffler M, Kartashov D, Midorikawa K, et al. Duration of an intense laser pulse can determine the breakage of multiple chemical bonds. *Sci Rep* (2015) 5:12877–11. doi:10.1038/srep12877

34. Dörner R, Mergel V, Jagutzki O, Spielberger L, Ullrich J, Moshammer R, et al. Cold target recoil ion momentum spectroscopy: A 'momentum microscope' to view atomic collision dynamics. *Phys Rep* (2000) 330:95–192. doi:10.1016/s0370-1573(99)00109-x

35. Roither S, Xie X, Kartashov D, Zhang L, Schöffler M, Xu H, et al. High energy proton ejection from hydrocarbon molecules driven by highly efficient field ionization. *Phys Rev Lett* (2011) 106:163001. doi:10.1103/PhysRevLett.106.163001

36. Stapelfeldt H, Seideman T. Colloquium: Aligning molecules with strong laser pulses. *Rev Mod Phys* (2003) 75:543–57. doi:10.1103/RevModPhys.75.543

37. Alnaser AS, Tong XM, Osipov T, Voss S, Maharjan CM, Shan B, et al. Laser-peak-intensity calibration using recoil-ion momentum imaging. *Phys Rev A* (2004) 70:023413. doi:10.1103/PhysRevA.70.023413

38. Nisoli M, De Silvestri S, Svelto O. Generation of high energy 10 fs pulses by a new pulse compression technique. *Appl Phys Lett* (1996) 68:2793–5. doi:10.1063/1.116609

39. Xie X, Doblhoff-Dier K, Roither S, Schöffler MS, Kartashov D, Xu H, et al. Attosecond-recollision-controlled selective fragmentation of polyatomic molecules. *Phys Rev Lett* (2012) 109:243001. doi:10.1103/PhysRevLett.109.243001

40. Sayler AM, Rathje T, Müller W, Rühle K, Kienberger R, Paulus GG. Precise, real-time, every-single-shot, carrier-envelope phase measurement of ultrashort laser pulses. *Opt Lett* (2011) 36:1–3. doi:10.1364/OL.36.000001

41. Relph RA, Bopp JC, Roscioli JR, Johnson MA. Structural characterization of (C2H2)1-6+ cluster ions by vibrational predissociation spectroscopy. *J Chem Phys* (2009) 131:114305. doi:10.1063/1.3212595

42. Jiang YH, Rudenko A, Herrwerth O, Foucar L, Kurka M, Kühnel KU, et al. Ultrafast extreme ultraviolet induced isomerization of acetylene cations. *Phys Rev Lett* (2010) 105:263002. doi:10.1103/PhysRevLett.105.263002

43. Ibrahim H, Wales B, Beaulieu S, Schmidt BE, Thiré N, Fowe EP, et al. Tabletop imaging of structural evolutions in chemical reactions demonstrated for the acetylene cation. *Nat Commun* (2014) 5:4422–8. doi:10.1038/ncomms5422

44. Hu H, Larimian S, Erattupuzha S, Wen J, Baltuška A, Kitzler-Zeiler M, et al. Laser-induced dissociative recombination of carbon dioxide. *Phys Rev Res* (2019) 1: 033152. doi:10.1103/PhysRevResearch.1.033152

45. Tong XM, Zhao ZX, Alnaser AS, Voss S, Cocke CL, Lin CD. Post ionization alignment of the fragmentation of molecules in an ultrashort intense laser field. *J Phys B: Mol Opt Phys* (2005) 38:333–41. doi:10.1088/0953-4075/38/4/002